UCRL- 92598 Rev. 2
PREPRINT

INSTABILITIES, TURBULENCE, AND THE PHYSICS OF FIXED POINTS

Minh Duong-van

Submitted to Springer-Verlag

January 1986

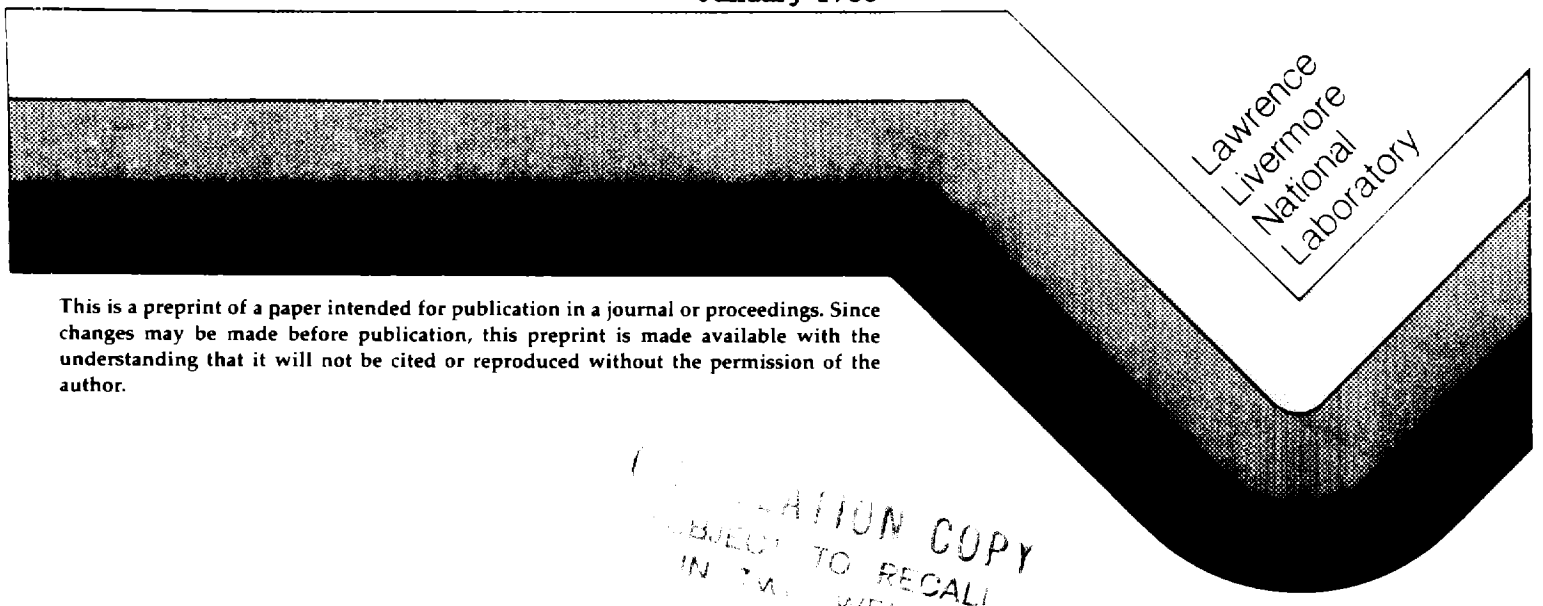

INSTABILITIES, TURBULENCE, AND THE PHYSICS OF FIXED POINTS*

Minh Duong-van

University of California

Lawrence Livermore National Laboratory

Livermore, CA 94550

ABSTRACT

We study a recursion relation that manifests two distinct routes to turbulence, both of which reproduce commonly observed phenomena: the Feigenbaum route, with period-doubling frequencies; and a much more general route with noncommensurate frequencies and frequency entrainment, and locking. Intermittency and large-scale aperiodic spatial patterns are reproduced in this new route. In the oscillatory instability regime the fractal dimension saturates at $D_F \approx 2.6$ with imbedding dimensions while in the turbulent regime D_F saturates at 6.0.

*This work was performed under the auspices of the U.S. Department of Energy by the Lawrence Livermore National Laboratory under contract number W-7405-ENG-48.

Experimental evidence supporting Feigenbaum's route to turbulence[1,2] has become richer since 1978. In this route, nonlinear systems manifest chaos via period– doubling bifurcations. For example, Rayleigh–Bénard systems with low[3,5] and intermediate[6] Prandtl numbers exhibit this route. In detailed experiments on low– aspect–ratio Rayleigh–Bénard cells, Giglio et al.[6] saw four period doublings and obtained values of δ that agree with Feigenbaum's[1] universal $\delta = 4.6692$ within their experimental error.

When the aspect ratio is large, however, very different behavior is found.[7–11] As the stress parameter (the Rayleigh number, in the case of Rayleigh–Bénard systems) is increased, cascades of instabilities are observed, each step of which adds new complications to the convective behavior.[3,8,10] Unstable patterns are formed and temporal chaos[8] sets in, with alternating random bursts and quietness: this is called intermittency.[3,8] Noncommensurate frequencies arise in the Fourier spectrum of the chaotic variable, and entrainment and locking occur as the stress parameter is varied.[3,7,8]

In this paper we show that both these routes to turbulence, with all the properties just described, can be simply simulated with a quadratic map at each site of a spatial lattice and with a coupling between nearest–neighbor sites. This new route leads to a fractal dimensions of 2.6 at the oscillatory instability regime and 6.0 at the turbulent regime.

Let u represent the chaotic variable: it may be a velocity component or a temperature fluctuation of the system being studied. We build a lattice of sites with a quadratic map $u \to Q(\lambda,u)$ at each site, and allow interaction between nearest neighbor sites through a coupling parameter g. We assign a random value of u to each lattice site, and let the lattice evolve in time steps $t_n = n\tau$, $n = 1, 2, 3 \ldots$, when τ is the Poincaré time of the system. We find the same behavior for all quadratic $Q(\lambda,u)$: for example,

$$Q(\lambda,u) = \lambda u(1-u), \tag{1a}$$

$$Q(\lambda,u) = \lambda\sin(\pi u) \tag{1b}$$

give the same behavior. For simplicity, we use the logistic map, Eq. (1a), in this study. In one dimension, we use the prescription[14,15]

$$u_{n+1}(m) = \lambda u_n(m)[1 - u_n(m)] + \frac{g}{2}[u_n(m+1) + u_n(m-1) - 2u_n(m)], \tag{2}$$

where the index m spans the N lattice points m = 1, 2, ...,N.

With Eq. (2) two routes to turbulence are observed, in which the Feigenbaum route is seen as a special case.

For small g (e.g., g ≃ 0.001), when λ approaches the accumulation point λ_∞, the Fourier spectrum of the time sequence $u_n(m)$ for a particular m shows period–doubling bifurcations.[1] (With $\lambda_\infty \simeq 3.569$ and g ≃ 0, for example, we obtain a period–doubling Fourier spectrum that agrees well with that obtained by Giglio et al.[6] As g increases, the peaks in the Fourier spectrum become wider. In our study, this width increase is a consequence of the dissipative term controlled by g. As λ increases to 4 (for <u>any</u> value of g) the spectrum becomes flat and chaotic.

Only in special cases (such as in Rayleigh–Bénard systems with low aspect ratio) does the turbulence observed in nature follow the Feigenbaum route. More generally (as in Rayleigh–Bénard systems with large aspect ratios), the instabilities and turbulence show richer behaviors.[7,11] One observes noncommensurate frequencies in the Fourier spectrum and the phenomena of frequency entrainment and locking; complex quasi–periodic, aperiodic, and intermittent time histories of the values of chaotic variables at individual points in the system; and similar time variations in the spatial patterns formed in certain systems.[3] By iterating Eq. (2) or (in the case of the spatial

patterns) with values of g away from zero, we can reproduce all these phenomena, provided we restrict λ to the Feigenbaum simple fixed points region $1 < \lambda < 3$.

We built a periodic one–dimensional lattice with N = 2000, and recorded the time evolution and the corresponding Fourier transform of u_n (13) for times up to $n = 2^{12}$ and for a variety of values of λ and g (m is arbitrarily chosen equal to 13).

For illustration, we choose g = 0.915 and vary λ from $\lambda_{max} = 1.621$ to $\lambda_{min} = 1.0$. Figure 1(a) ($\lambda = 1.62$) shows the Fourier spectrum and the time history of u_n. This broad spectrum, with its intermittent bursts and quietness, appears to correspond to observations described in Ref. 3. In Fig. 1(b) ($\lambda = 1.52$) the frequency peaks become narrower, and the amplitude variations become smaller.

In Fig. 2(a) ($\lambda = 1.449$), the time history shows that the system attempts to settle to the fixed point ($u^* = 1 - 1/\lambda$) after some transient time. The competition between the approach to the fixed point (due to λ) and the diffusion away from the fixed point (due to g) gives rise to the instability observed. In Fig. 2(a) ($\lambda = 1.449$) the Fourier spectrum exhibits noncommensurate frequencies.

As λ is decreased further, the frequencies are entrained (Fig. 2(b) $\lambda = 1.49$) and locked (Fig. 3(a) $\lambda = 1.48$).

We generate visible patterns with the two–dimensional by use of a new graphical technique,[17] scaling the u(j,k) to a 0–to–256 linear gray scale.

In the simulation of these patterns, the u(j,k) are assigned initial (n = 1) random values between 0 and 1, resulting at most in small–scale random patterns at that time. As time increases, these patterns disappear into a highly uniform sea (when u_n approaches the fixed point); eventually, however, large–scale structures grow, evolve, and temporarily or permanently stabilize. Fig. 4 shows the pattern developed in a 50x50 lattice for $\lambda = 1.5$, g = .905.

We have chosen to study only the simple fixed points region $1 < \lambda < 3$ of the logistic map, Eq. (2a). (In other regions, only random patterns are observed.) As long as g = 0,

this branch produces uninteresting behavior: the u_n approach the fixed point $u^* = 1 - 1/\lambda$. Without g, there is no instability in this region, and no patterns. When we turn g on, however, depending on the values of g and λ, we may we get rich and interesting behaviors clearly, in Figs. 1 and 2, g acts to keep the u_n from their tendency toward the fixed point. Thus instabilities appear to result from a competition between tendencies towards the fixed points and away from it, and the time history intermittency phenomenon (Fig. 1a) is, in fact, a consequence of this competition.

Influenced by the recent measurements of the fractal dimension in periodically excited air jet by Bonetti et al.[17] and in an electron-hole plasma in Ge by Held and Jeffries,[18] we calculate the fractal dimension of our system in the oscillatory instability regime (Figs. 2b, 3a) and turbulent regime (Fig. 1a) and we found $D_F \simeq 2.6$ and 6.0 respectively. From the set of data $u_n(m)$ where n = 3000 and the lattice site m varies from 1 to 500, we constructed $m_{max} - D + 1$ vectors $G^m = (u^m, u^{m+1}, \ldots, u^{m+D-1})$ in a D-dimensional phase space; D is referred as the imbedding dimension of the reconstructed phase space G. Note that the coordinates in our reconstructed phase space correspond to different lattice sites and not to time delays. Next, we compute the number of points on the attractor, N(R), which are contained in a D-dimensional hypersphere of radius R. If one considers the fractal dimension a critical index of a critical phenomenon, one expects at the critical point, N(R) to scale as R^{D_F} where D_F is the fractal dimension of the attractor. This procedure is carried out for consecutive values D = 2,3,4 ..., to insure the D to be sufficiently large. We found that for g = .915, $1.47 < \lambda < 1.49$ (around the phase lock regime) the fractal dimension is roughly 2.6. In the turbulent regime, g = .915, λ = 1.62, $D_F \simeq 6.0$. The D_F for the first case stabilizes to 2.6 at $D \simeq 20$ while for the latter case, D_F is hard to calculate even at D = 30. This difficulty was also experienced by Bonetti et al.[17] and Atten et al.[19] The most interesting phenomenon observed here is the existence of a parametric transition of the D_F from 0.5 at $\lambda < 1.47$ to $D_F \simeq 2.6$ at $1.47 < \lambda < 1.49$. Figure 5 shows D_F versus λ at a given g. The universal value of

$D_F \approx 2.6$ observed experimentally is a consequence of the quadratic property of the logistic map. We have repeated the calculation with a 2–dimensional lattice, and varied the time delay and also the lattice size to 2000. Within the errors, the fractal dimension does not change significantly. In this paper, the errors are simply estimated by fitting to the slopes of the Log N(R) versus Log R curves. We observe a change of the width of the plateau at $D_F \approx 2.6$ with the size of the lattice. For 300 sites, the plateau width spans from $1.46 < \lambda < 1.51$ and for 2000 sites, the plateau width narrows down to $1.48 < \lambda < 1.49$. From the trend, one might speculate that in the continuum limit, the transition from $D_F \approx 0$ to a large fractal dimension (in the turbulent regime) might be continuous. Further investigations of this phenomenon and the detailed errors calculations are presently carried out.

In conclusion, we note that the variety of phenomena experimentally observed in the approach to turbulence has brought forth a variety of explanations: for example, intermittency can be explained[18] by the Lorenz model; the lock–in phenomenon can be explained by the Flaherty and Hoppensteadt model.[19] In our model, by putting the quadratic map on the lattice with nearest neighbors coupling, we economically recover all these phenomena. Furthermore, we have found that the common fractal dimension of 2.6 is a consequence of the quadratic map.

The author thanks P. R. Keller for the graphics used in this paper nd P. W. Murphy for editorial assistance. He thanks his colleagues at Lawrence Livermore and Los Alamos National Laboratories for numerous profitable discussions. Valuable suggestions and comments by C. Alonso, P. Carruthers, P. Cvitanovic and M. Feigenbaum are appreciated. He also thanks the Aspen Institute for Physics for their hospitality and the participants for stimulating discussions.

REFERENCES

1. M. J. Feigenbaum, Phys. Lett. 74A, 375 (1959). I thank P. Cvitanovic for providing me with information on a more comprehensive survey of recent data on this phenomenon. Also, Universality in Chaos, P. Cvitanovic, Ed. (Adam Hilger Ltd., Bristol, England, 1984), p. 29.
2. M. J. Feigenbaum, Comm. Math. Phys. 77, 65 (1980).
3. J. Maurer and A. Libchaber, J. Phys. Lett. 40, L-419 (1979); and Universality in Chaos, P. Cvitanovic, Ed. (Adam Hilger Ltd., Bristol, England, 1984), p. 109.
4. A. Libchaber and J. Maurer, J. Phys. Colloq. 41, C3-51 (1980).
5. P. S. Linsay, Phys. Rev. Lett. 47, 1349 (1981).
6. M. Giglio, S. Musazzi, and V. Perini, Phys. Rev. Lett. 47, 243 (1981).
7. J. P. Gollub and S. A. Benson, Phys. Rev. Lett. 41, 948 (1978).
8. M. Dubois and P. Bergé, J. Fluid, Mech. 85, 641 (1978), and Systems Far From Equilibrium, L. Garrido, Ed. (Springer-Verlag, New York, 1980), p. 381.
9. G. Ahlers and R. W. Walden, Phys. Rev. Lett. 44 445 (1980); Phys. Lett. 76A, 53 (1980).
10. G. Ahlers and P. R. Behringer, Supp. Prog. Theor. Phys. 64, 186 (1978).
11. J. Maurer and A. Libchaber, J. Phys. Lett. 41, 515 (1980).
12. K. Kaneko, Prog. Theor. Phys. 69 1427 (1983); Prog. Theor. Phys. 72, 480 (1984).
13. I. Waller and R. Kapral, Phys. Rev. A 30, 2047 (1984).
14. Minh Duong-van and P. R. Keller, "Pattern Formation in Spinodal and Phase Turbulent Instabilities," Lawrence Livermore National Laboratory, Livermore, CA, UCRL-92716 (1985).
15. P. Berge, M. Dubois, P. Mannville and Y. Pomeau, J. Physique-Lettres 41, L-341 (1980).

16. J. E. Flaherty and F. C. Hoppensteadt, Study Appl. Math., 58, 5 (1978).

17. M. Bonetti et al., PRL 55, 492 (1985).

18. G. A. Held and Carson Jeffries, PRL 55, 887 (1985).

19. P. Atten et al., "Determination of Attraction Dimension for Various Flows," to be published.

FIGURE CAPTIONS

Figure 1. (Top to bottom: Fourier spectrum of u_n; u_n; and enlargement of indicated portion of u_n.) (a) $g = 0.915$, $\lambda = 1.62$; (b) $\lambda = 1.52$.

Figure 2. (Same plots as in Fig. 1.) (a) $g = 0.915$, $\lambda = 1.499$; (b) $\lambda = 1.490$.

Figure 3. (Same plots as in Fig. 1.) (a) $g = 0.915$, $\lambda = 1.48$; (b) $\lambda = 1.00$.

Figure 4. Patterns generated by a 50 x 50 lattice with $\lambda = 1.50$, $g = .905$ and $n = 90$.

Figure 5. Fractal dimension variation as a function of the parameter λ at a fixed $g = .915$. Detailed features of the parametric transition at $\lambda = 1.47$ should be complemented by refering to Figs. 1a–3b.

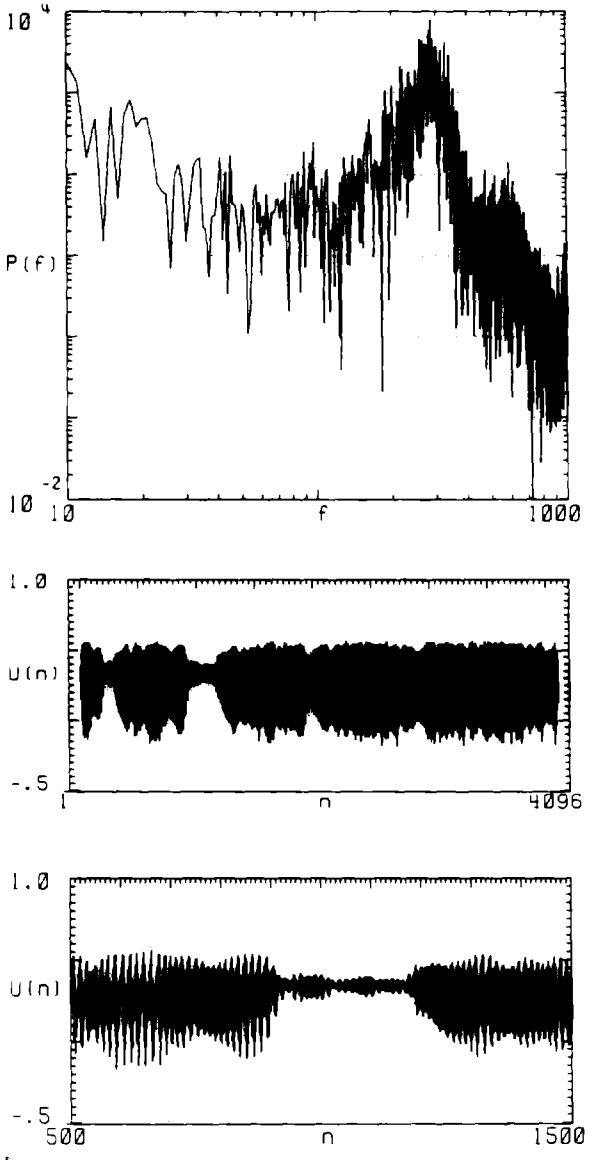
10 4
P(f)
10 -2
10
f
1000
1.0
U(n)
-.5
1
n
4096
1.0
U(n)
-.5
500
n
1500

Fig. 1a

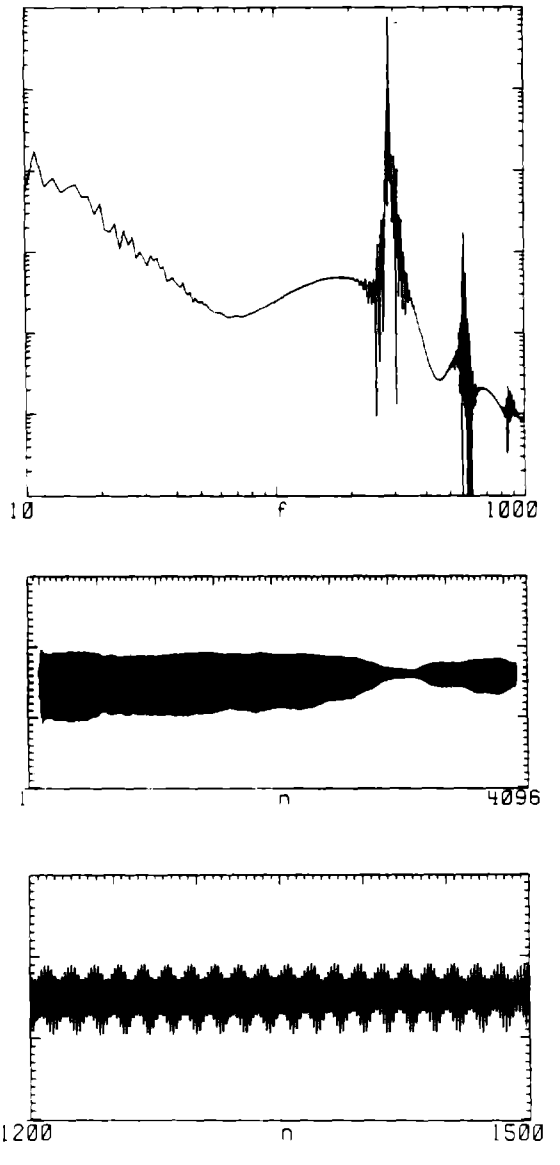
10
f
1000
1
n
4096
1200
n
1500

Fig. 1b

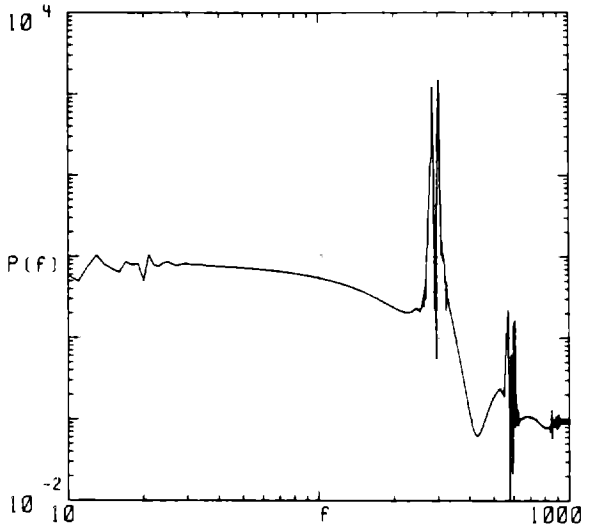
10 4
P(f)
10 -2
10
f
1000

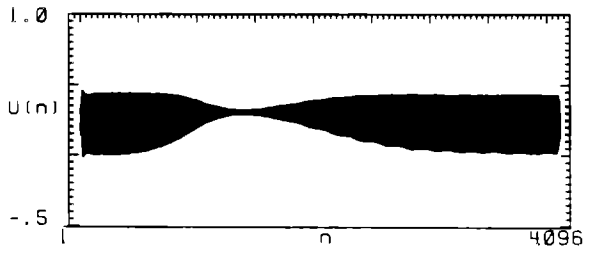
1.0
U(n)
-.5
1
n
4096

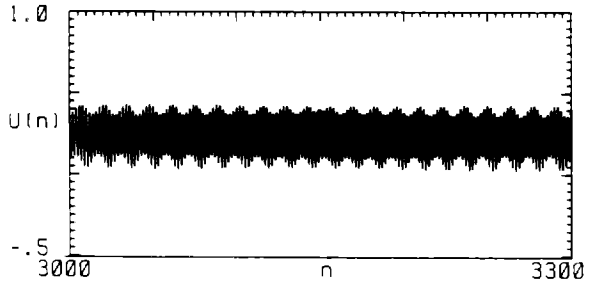
1.0
U(n)
-.5
3000
n
3300

Fig. 2a

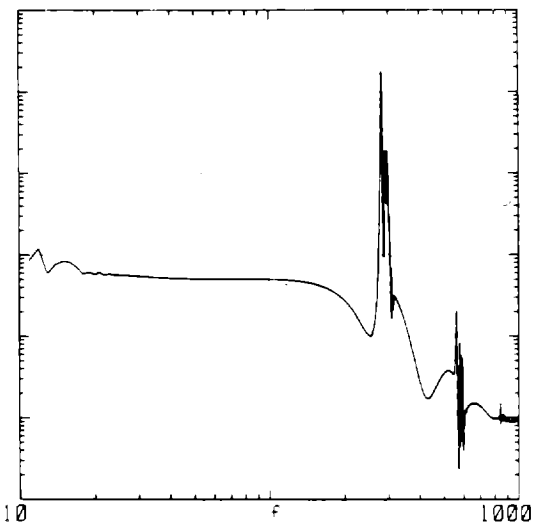
10
f
1000

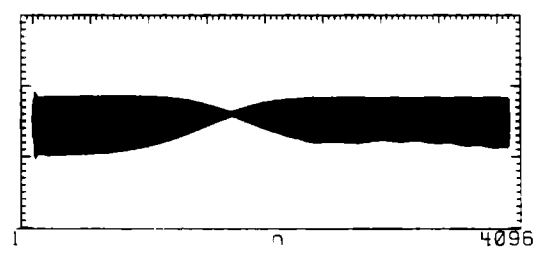
1
n
4096

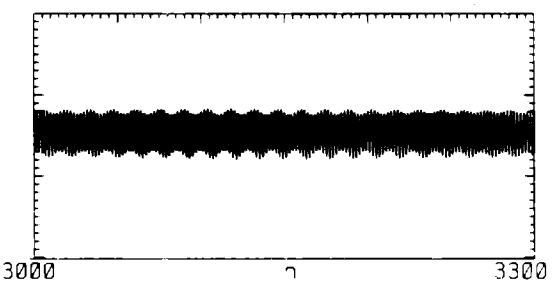
3000
n
3300

Fig. 2b

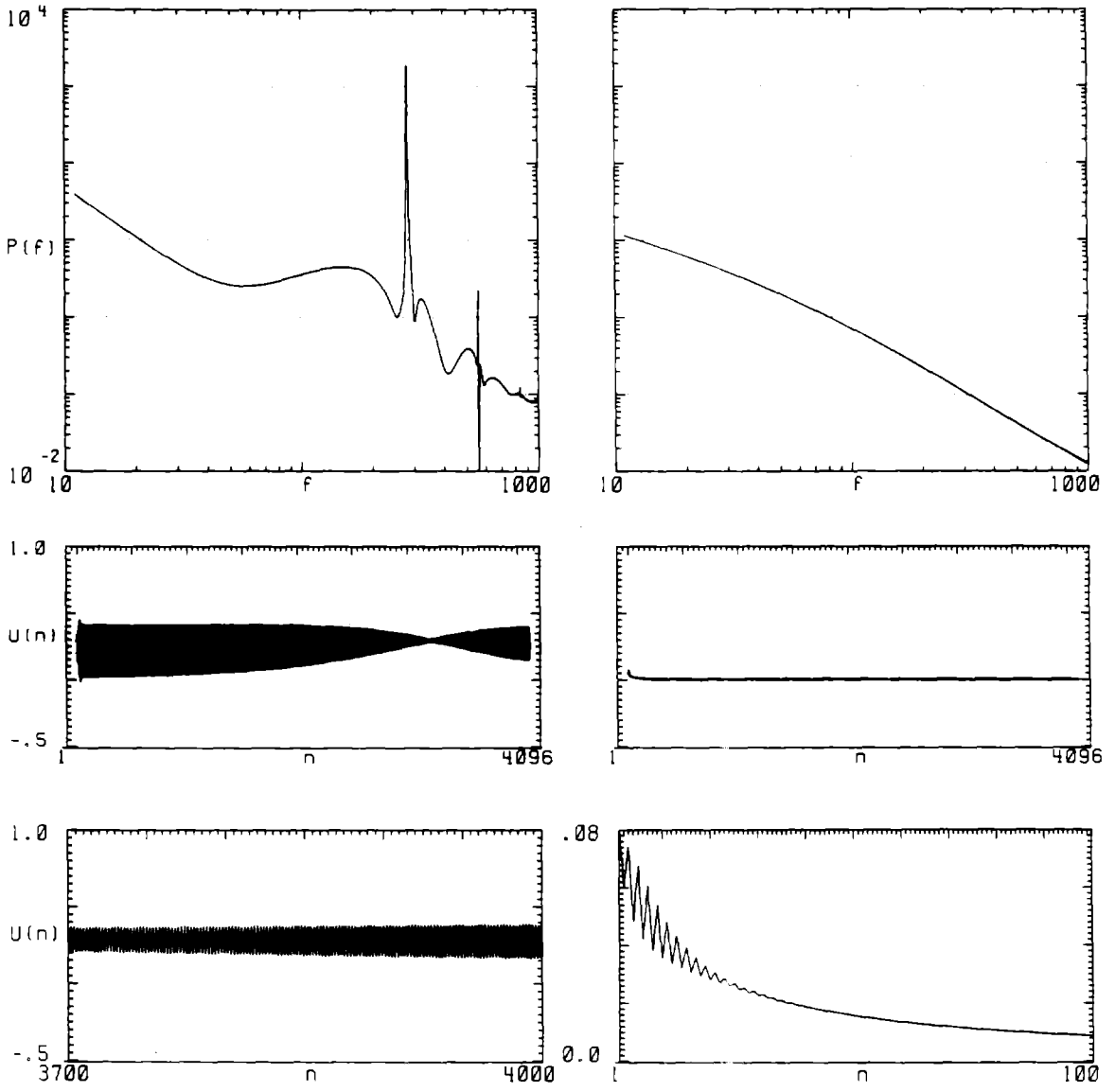

Fig. 3a

Fig. 3b

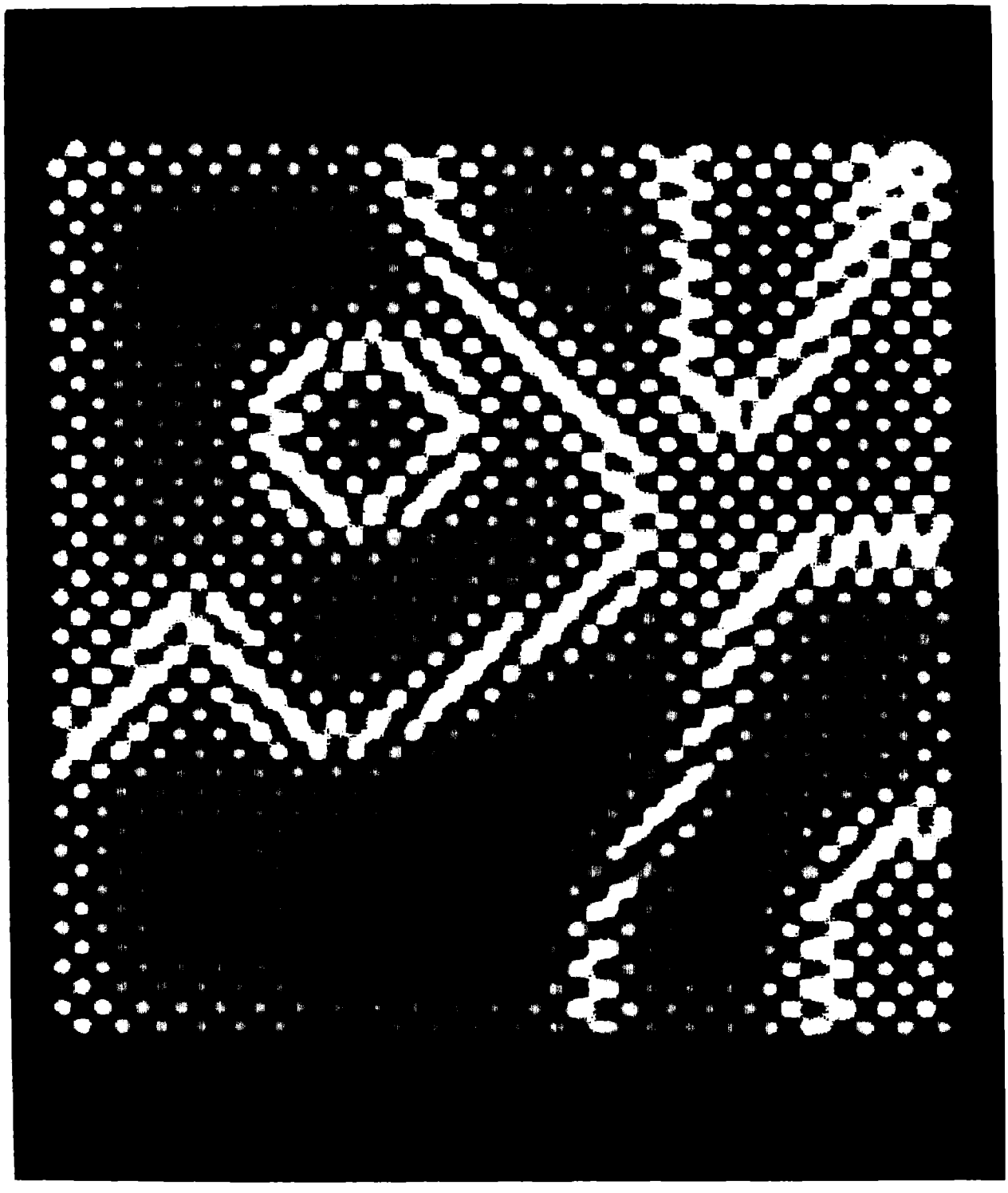

Fig. 4

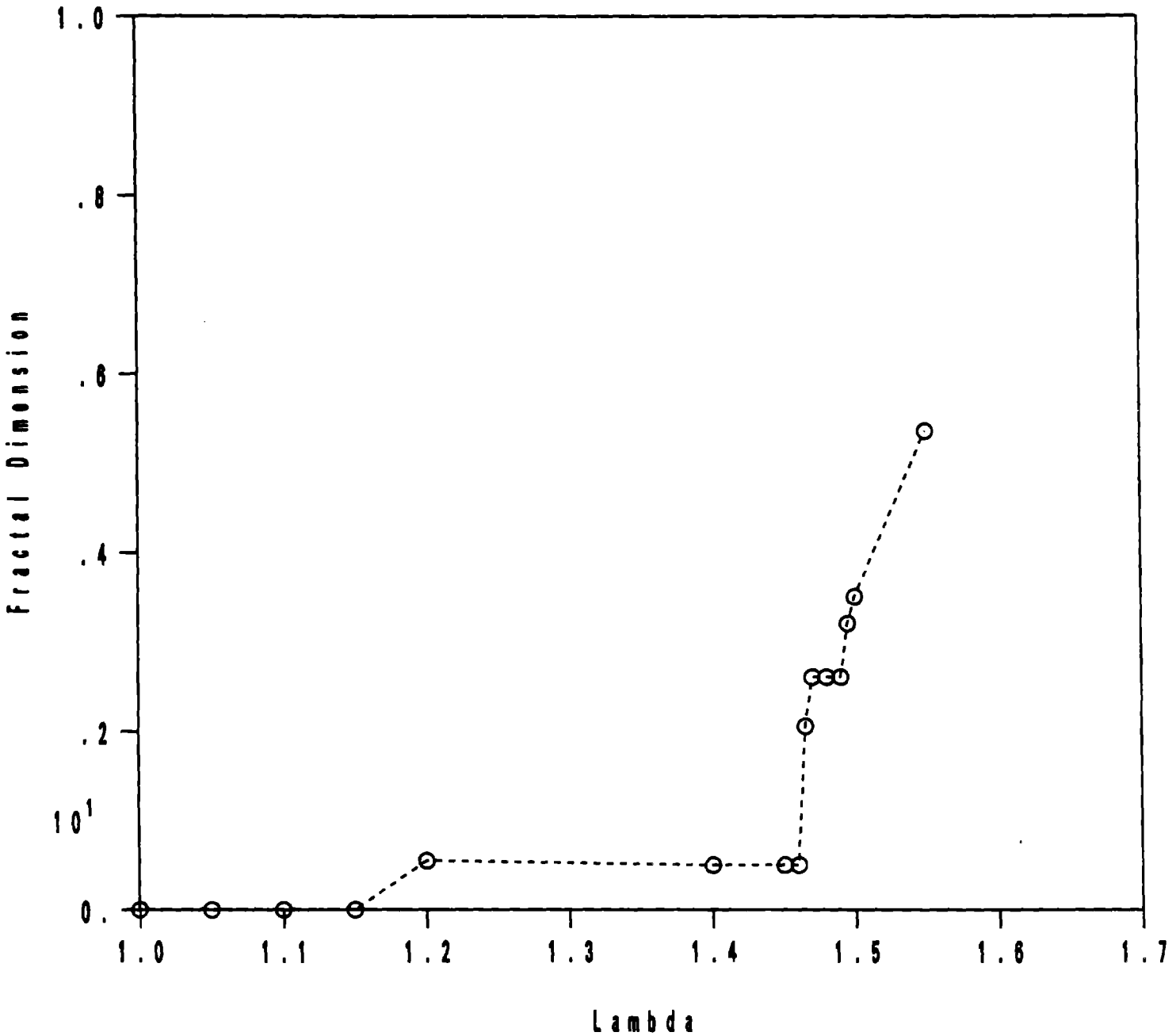

Fig. 5